


In situ XRPD study of the ambient-pressure synthesis of nonstoichiometric Ag₃O from Ag–Ag₂O thin films: Phase abundance, unit-cell parameters, and *c/a* as a function of temperature and time

Paul J. Schields ^{1,a)} Nicholas Dunwoody,² David Field,³ and Zachary Wilson⁴

¹Albany Molecular Research Inc., West Lafayette, IN 47906, USA

²Tetraphase Pharmaceuticals, Inc., Watertown, MA 02472, USA

³Calgary, AB, Canada T2M 0E

⁴Groton, MA 01450, USA

(Received 29 June 2020; accepted 21 August 2020)

Ag₃O was synthesized by jet-milling magnetron-sputtered Ag–Ag₂O thin films. Heating the jet-milled powders in air and N₂ from 40 to 148 °C at ambient pressure produced Ag₃O-rich powders. The phase composition and unit-cell parameters of the jet-milled powders were measured as a function of temperature with *in situ* X-ray powder diffraction experiments from –186 to 293 °C. Ag₃O was also produced by ball milling and sonicating jet-milled films at ambient conditions. The phase composition, unit-cell parameters, and thermal-reaction rates indicate nonstoichiometric Ag₃O was produced from the reaction of metastable, nonstoichiometric Ag₂O (cuprite structure) and ccp Ag. The thermal expansion of Ag₃O is anisotropic; below 25 °C, the *a*-axis expansion is about twice the *c*-axis expansion resulting in a negative slope of *c/a*(*T*). The reversal of the sign of *c/a*(*T*) near 25 °C is dramatic. The thermal reaction is arrested when the temperature is rapidly increased from ambient to 130 °C. Ag₃O is metastable and decreases its unit-cell volume during kinetic decomposition to Ag when heated above ambient temperature in air and nitrogen. The relative volume expansion of Ag₃O is about 80% less than Ag at room temperature and below. The suite of nonstoichiometric Ag₃O produced by heating displays a linear relation between *c/a* and unit-cell volume at room temperature. The *c/a* and unit-cell volume of a hydrothermally grown Ag₃O single crystal reported in a published structure determination was the Ag-rich, low-volume end member of the linear series. The *c/a* and unit-cell volume are sensitive indicators of the oxygen content and state of disorder. © 2020 International Centre for Diffraction Data. [doi:10.1017/S0885715620000561]

Key words: Ag₃O, Ag₂O, Ag, *in situ* thermal reaction, thermal expansion, nonstoichiometry, XRPD

I. INTRODUCTION

The crystal structure of Ag₃O was determined by Beesk *et al.* (1981) using XRD on a crystal grown by the hydrothermal reaction of AgO on a Ag substrate at 4 kbar for several days.¹ No other published study has identified Ag₃O prior to the present study. The structure consists of a sublattice of hexagonal closest-packed (hcp) Ag with a two-layer repeat and oxygen occupying two-thirds of the octahedral interstices in every other adjacent closest-packed layer [Figures 1(a) and 1(b)].

Prior to the Ag₃O structure determination, X-ray powder diffraction (XRPD) patterns of silver oxide powders produced at 115–125 kbar and 1100–1400 °C were reported as “Ag₂O II” and “high-pressure modification” by Kabalnikina *et al.* (1963). The Ag₂O II crystal structure was described as hcp

Ag with oxygen occupying *all* octahedral interstices in every other adjacent, cp layer; this layered structure is isostructural with Ag₂F, an inverse-CdI₂ structure type. Similar powder patterns were reported by Birkenberg and Schwarzmann (1974) for “hexagonal Ag₂O” synthesized by hydrothermal reactions of AgO and Ag₂O on Ag substrates for 6 weeks at 3.7 kbar and temperature gradients from 79 to 52 °C.

Beesk *et al.* (1981) found the hexagonal unit cell reported for Ag₂O II at ambient conditions was a subcell of their Ag₃O *P* $\bar{3}$ 1 *m* cell with *a* = 5.318(2) Å and *c* = 4.951(2) Å where the *a* axis is $\sqrt{3}$ times the *a* axis of the subcell and is rotated by 60° around the subcell *c* axis. Weak peaks generated by the ordered occupation of oxygen in two-thirds of the octahedral interstices in Ag₃O were not observed in the Debye–Scherrer patterns of the material synthesized in the high-pressure and hydrothermal experiments. However, the very low signal-to-background in the published Debye–Scherrer images would have obscured these weak peaks if present.

In the present study, a suite of Ag₃O-rich powders was synthesized by heating jet-milled, magnetron-sputtered films from room temperature to 148 °C at atmospheric pressure in an atmosphere composed of either ambient air or N₂ for time periods from hours to several years. The reactant jet-milled films were composed of a majority of Ag₂O with the

^{a)} Author to whom correspondence should be addressed. Electronic mail: paul.schiels@amriglobal.com

¹ The only temperature reported by Beesk *et al.* was 80 °C; we presume this was the temperature *gradient* because it is similar in magnitude to the gradients reported by Birkenberg and Schwarzmann (1974). The temperature of the reaction is expected to be several-hundred °C to generate a pressure of 4 kba

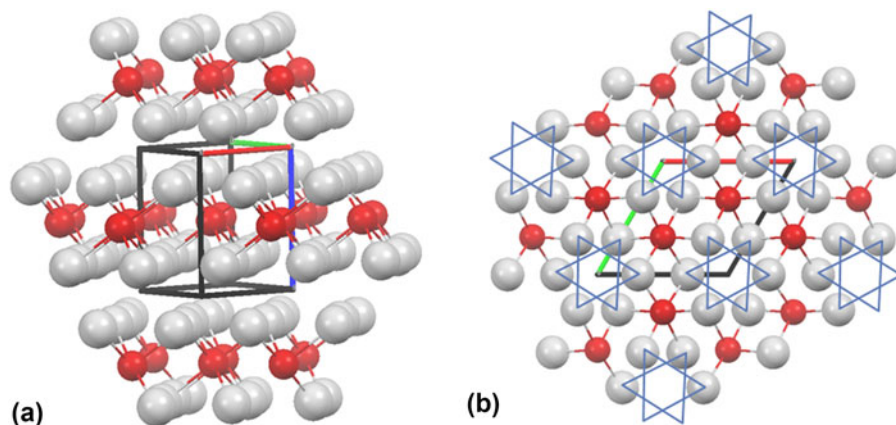


Figure 1. (Color online) The structure of Ag_3O determined by Beesk *et al.* (1981); light (grey) spheres are hcp Ag and dark (red) spheres are oxygen; the a axis is red, the b axis is green, and the c axis is blue. (a) Perspective view and (b) c axis projection showing the tunnels formed by the empty octahedral interstices sharing rotated trigonal faces (blue).

cuprite structure and ccp Ag, as well as a minor amount of Ag_3O . Ag_3O was also produced from the jet-milled powders by ball milling and by sonication. The phase composition and unit-cell parameters of these products were measured with *in situ* and *ex situ* experiments from -186 to 293 °C as a function of temperature and time. The thermal reaction was studied as a function of time at 100 and 130 °C.

II. EXPERIMENTAL

A. Physical vapor deposition and jet-milling of the reactant thin film

Ag_3O powders were synthesized by heating jet-milled films composed of a mixture of Ag_2O and ccp Ag in air and nitrogen. The films were provided by NUCRYST Pharmaceuticals Inc. and were grown by reactive, direct-current, magnetron sputtering of silver (99.99 wt%) onto stainless steel. The atmosphere was composed of approximately 2 vol% oxygen and 98 vol% argon, with a nominal pressure of 5.3×10^{-5} atm and gas-flow rates for Ar and O_2 of 7400 and 160 standard $\text{cm}^3 \text{min}^{-1}$, respectively. The temperature of the stainless-steel substrate was 35 ± 3 °C. The films were removed from the stainless-steel substrate by scraping with a stainless-steel blade.

The removed films were jet milled using a Micron-Master 8" orbital jet mill by Jet Pulverizer Company. Compressed ambient air was used for jet milling. Jet-milled films were used as reactants (Table I) to produce the samples described in Table II. U1 and U2 were products from reactant thin films similar to those included in Table I; however, the phase composition of these films was unavailable.

TABLE I. Estimated phase compositions of jet-milled films.

Reactant film #	Ag (wt%)	Ag_2O (wt%)	Ag_3O (wt%)	Ag/ Ag_2O molar ratio
1	42	47	11	1.9
2	34	65	Not detected	1.1
3	44	48	8	2.0

B. Diffractometer configuration and *in situ* temperature correction

XRPD patterns were collected using transmission and Bragg–Brentano configurations of Panalytical X'Pert Pro MPD and Epyrean diffractometers. $\text{CuK}\alpha$ X-rays generated at 45 kV and 40 mA were focused on an X'Celerator detector using an elliptically graded W/Si multilayer mirror for the transmission configuration. Transmission specimens were packed between thin polymer films. The Bragg–Brentano configuration used a Ni filter, an X'Celerator, fixed slits (0.125° divergence, 0.25° incident-beam antiscatter, and 5.0 mm diffracted-beam antiscatter), and specimens packed in a 0.2-mm well in a silicon zero-background holder.

In situ heating and cooling experiments were completed with Anton Paar TTK 450 and THC stages in Bragg–Brentano configuration. The temperature of the specimen

TABLE II. *Ex situ* reaction-product identifications, reaction times, temperatures and atmospheres, and estimated phase compositions of thermally reacted, sonicated, and ball-milled reactant films.

Product ID	T (°C), atmosphere	time (t)	Ag (wt%)	Ag_2O (wt%)	Ag_3O (wt%)
1a	130, air	4 days	48	2	50
1b	100, air	2 days	16	1	84
1c	141, N_2	6 days	35	Not detected (ND)	65
1d	60, air	11 wk	19	<1	81
1e	60, air	1 yr	22	ND	78
2a	100, air	Unavailable	3	19	78
3a	100, air	1 wk	14	3	83
3b	100, air	2 wk	18	1	81
3c	40, air	28 mo	15	ND	85
3d	120, air	4 wk	25	<1	75
1 sonicated	Ambient	3 min	75	<1	25
1 sonicated cyclohexane	Ambient	45 s	85	<1	15
1 sonicated IPA	Ambient	90 min	24	ND	76
B1 ball milled	Ambient	90 min	24	ND	76
B1 a	80, air	1 day	31	ND	69
B1 b	100, air	1 day	33	ND	67
B1 c	120, air	1 day	35	ND	65
B1 d	150, air	5 days	100	ND	ND
U1	Unavailable	Unavailable	1	5	94
U2	40, air	15 mo	1	8	91

was measured using a 100 Ω platinum resistive-temperature probe (Pt-100) positioned in a nickel-coated copper holder under the specimen well. A thin layer of heat-conducting grease was applied to the bottom of the holder. Humidity for *in situ* experiments was measured with an HC2-C05 capacitive humidity probe housing a Pt-100 sensor in the THC chamber. Data was displayed by a Rotronic HF5 transmitter. Humidity was generated by a VTI RH-200.

Temperatures above ambient were corrected using *in situ* XRPD of several organic melting-point standards and the thermal expansion of Ag metal determined by Suh *et al.* (1988) from 25 to 1228 $^{\circ}\text{C}$ using XRPD (Supplementary Figure S1). To account for the current $\text{CuK}\alpha_1$ used for whole-pattern refinements (section II.C), the thermal-expansion reference value for Ag at 25 $^{\circ}\text{C}$ was the average Ag unit-cell length 4.0865404 \AA from Yoder-Short (1993) rescaled to 4.086527 \AA by a multiplication factor of $0.9999966 = 1.5405929$ (current $\text{CuK}\alpha_1$) \div 1.5405981 (Yoder-Short, 1993).

Temperatures below room temperature were calibrated using the reversible and sharp transformation of ammonium sulfate from space group $Pnam$ at room temperature to $Pna2_1$ at -50.0 $^{\circ}\text{C}$ (Supplementary Figure S2; Schlemper and Hamilton 1966; Kosova *et al.*, 2014). Low temperatures were also calibrated using adamantane which transforms from ccp at room temperature to tetragonal at -65.2 $^{\circ}\text{C}$ (Supplementary Figures S3 and S4; Nordman and Schmitkons, 1965; van Ekeren *et al.*, 2006). The maximum correction of 3 $^{\circ}\text{C}$ for the lowest temperature observed in the present study, 189 $^{\circ}\text{C}$, was extrapolated from a quadratic regression (Supplementary Figure S1).

C. Whole-pattern refinement

XRPD patterns were processed using TOPAS V4.2 (Kern *et al.*, 2004; Bruker-AXS, 2009). Unit-cell parameters were

determined using converged Pawley (1981) refinements. The “CuKa2.lam” emission profile was used with updated values of $\text{CuK}\alpha_1$ (1.5405929 \AA) and $\text{K}\alpha_2$ (1.5444274 \AA) from Table IV of Hölzer *et al.* (1997). Phase compositions of the jet-milled films and samples synthesized by the thermal reaction of these powders (Table II) were estimated using the known crystal structure of each phase in converged whole-pattern refinements with TOPAS.

The phase compositions are estimated values because the anisotropic thermal parameters for Ag_3O have not been published and could not be reliably refined; they were approximated using isotropic parameter $B_{\text{eq}} = 1$ for oxygen and silver. Furthermore, the phase compositions are estimates because the nature of point defects and their effect on site occupations is unknown for Ag_3O and Ag_2O . Figures of the refined patterns from TOPAS include color-coded tick marks to indicate the hkl angles for each phase corresponding to the color-coded empirical formula shown in the legend.

For powder patterns collected as a function of temperature and time, the initial values of refined variables were taken from refinements of patterns adjacent in time, forward and backward, except for the first pattern collected in the *in situ* experiment which has initial values based on all of the refinements in the study. The uncertainty of phase abundance was qualitatively estimated from the typical variations of wt% observed when slightly different initial values and sequences of refining the same set of variables resulted in convergence with similar goodness of fits (GoFs).

For each experiment, the $0^{\circ} 2\theta$ angle was either measured or refined. Sample displacement was refined as a function of $\cos\theta$ for patterns collected in Bragg–Brentano configuration and as a function of $\sin\theta$ for patterns collected in transmission geometry. The PV_TCHZ peak-profile function was used with the variables u , v , w , and x either refined or determined from SRM 640e Si and SRM 660a LaB_6 refinements. The profile variables y and z were fixed at zero. The crystal size and strain

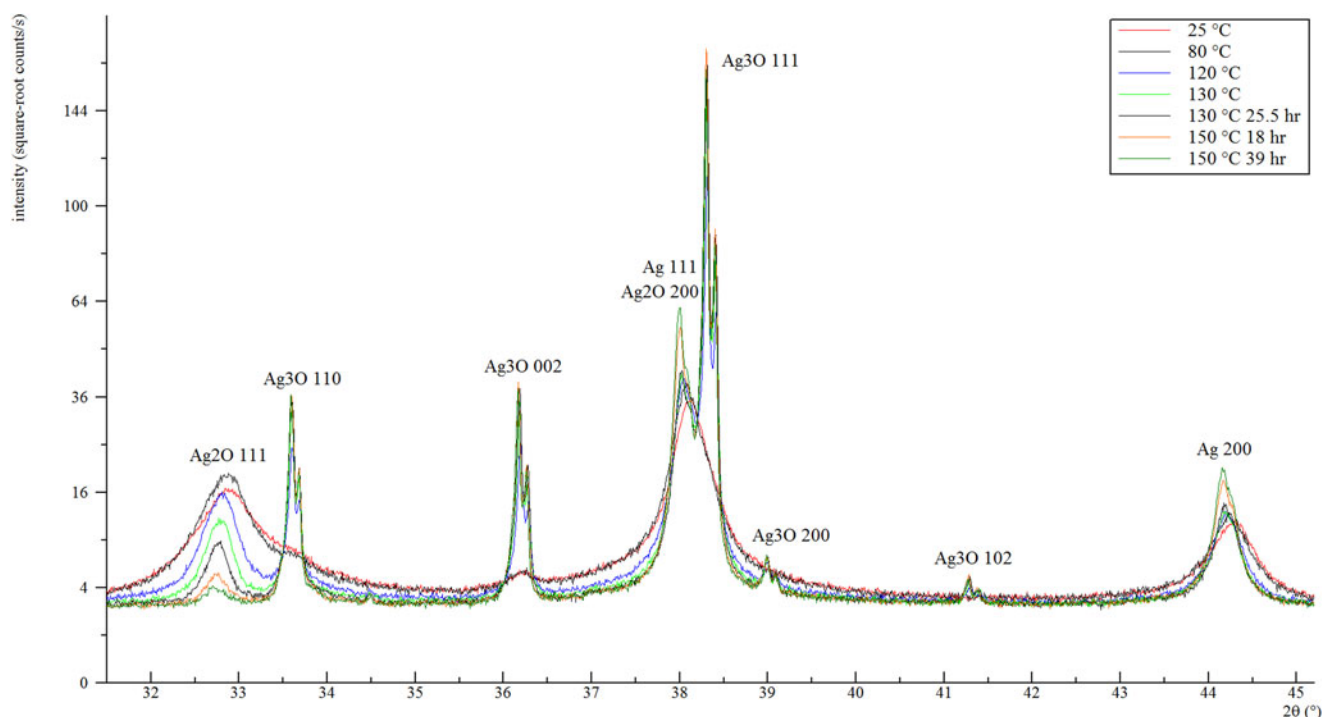


Figure 2. (Color online) Overlays of *in situ* XRPD patterns of film 1 heated in N_2 from 25 to 150 $^{\circ}\text{C}$.

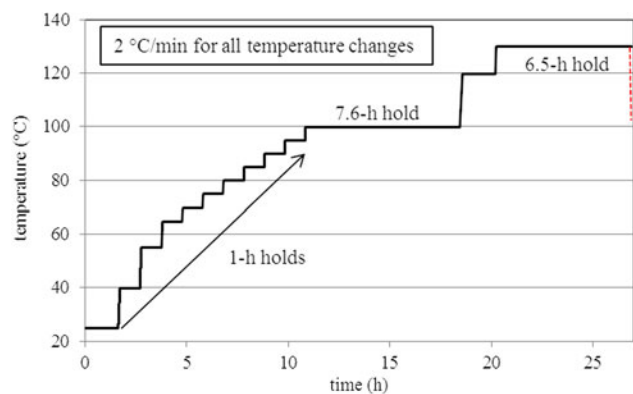


Figure 3. The temperature-time course for the thermal reaction of film 1 in N_2 from 25 to 130 °C. After the 6.5-hour hold at 130 °C heating continued at 130 °C for 25.5 h, and then 150 °C for 18 and 39 h.

were refined using Lorentzian and Gaussian profiles as needed for the best fit. Diffuse scattering was modeled using a “peaks phase” with a profile selected to provide the best fit to the Bragg peaks. The background signal was modeled using a 3rd-order Chebyshev and $1/X$ functions.

D. Ball milling parameters and *ex situ* heating

An MM 200 Retch Mixer Mill was used to ball mill film 1 (B1) at 30 Hz for 90 min in air at 50% RH with an approximately 100 mg sample spiked with a couple wt% SRM 640d Si. The mill and sample were noticeably warmed by milling; their temperatures were not monitored. After milling, the mill was allowed to cool for 2 h before the specimen was transferred to ambient temperature. The entire sample was heated *ex situ* to 80, 100, 120, and 150 °C in air and cooled to ambient at ≤ 1 °C min^{-1} after each heating. XRPD patterns were collected after each heat treatment at ambient conditions.

E. Sonication parameters

Approximately 0.5 g of jet-milled film 1 was sonicated at room temperature in a 4 ml suspension with isopropyl alcohol (IPA) for 45 s, and 1 g of jet-milled film 1 was sonicated in a 10 ml suspension with cyclohexane for 3 min. The sonication experiments used a Cole Parmer model CV18 probe operated between 6 and 12 W at ambient conditions.

III. RESULTS

The thermal-reaction products of jet-milled film 1 were analyzed *in situ* and *ex situ*. The thermal-reaction products of films 2 and 3 were analyzed *ex situ* in an ambient atmosphere. The amount of Ag_2CO_3 in the jet-milled films was determined by potentiometric acid-base titration to be approximately ≤ 10 wt% depending on the time (t) and temperature (T) of exposure to ambient air. The identification and phase compositions of the three reactant films are provided in Table I; these compositions excluded Ag_2CO_3 and were normalized to 100%. The identification, reaction conditions, and phase compositions of the synthesized samples are provided in Table II.

A. *In situ* thermal reaction of film 1 from 25 to 148 °C

In situ XRPD patterns were collected on jet-milled film 1 heated from 25 to 148 °C in N_2 flowing at 100 standard $cm^3 min^{-1}$

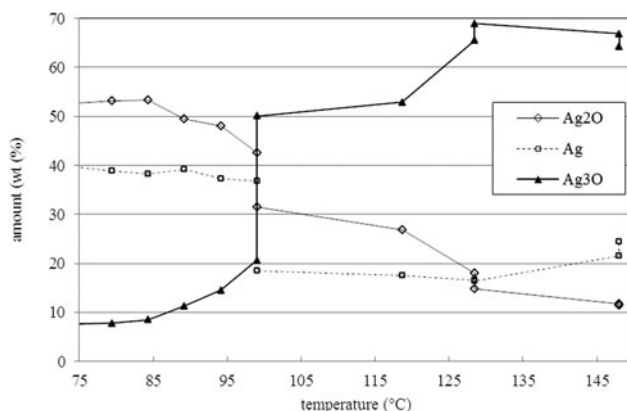


Figure 4. The estimated phase abundances as a function of temperature for the *in situ* thermal reaction of film 1 heated in N_2 .

(Figure 2). The temperature-time course for the first part of the experiment is shown in Figure 3; heating continued at 130 °C for 25.5 h and 148 °C for 18 h and then 39 h. A brief decrease in temperature to 102 °C occurred between the 6.5 and 25.5 h holds at the 130 °C target over a 2-min period. Patterns were collected over a 2θ range from 30 to 59° for 15 min at the end of each temperature hold. The ramp rate between temperature holds was 2 °C min^{-1} .

The estimated abundance of phases as a function of temperature is shown in Figure 4 starting at 80 °C, just before the reaction of Ag_2O and Ag starts to be detected at 90 °C. The lines through the data points are provided for visual guidance. The abundances for samples heated ≤ 80 °C were the same as the abundances at 80 °C, within the estimated uncertainty of ± 2 wt%.

Pawley refinements for patterns at 25, 80, and 120 °C are shown in Figure 5. The GoFs for all refinements of the *in situ* reaction products ranged from 1.1 to 1.35; R_{wp} ranged from 3.7 to 5.1. Diffuse scattering under the strong Bragg peaks was present in all of the patterns and was modeled as a “peaks phase” with maxima near 34.0, 37.5, and 44.0° displayed below the XRPD pattern. The unit-cell length of Ag_2O as a function of temperature, $a(T)$, is displayed in Figure 6 along with the time for each temperature hold.

B. *In situ* thermal-reaction kinetics of film 1 at 100 and 130 °C

The thermal reaction of jet-milled film 1 was analyzed *in situ* near a relative humidity of 100% at 100 °C in N_2 as a function of time (Figure 7). The estimated phase abundances expressed as mol% are shown in Figure 8. *In situ* patterns of another sample of film 1 were also collected every 41 s for 42 h at 130 °C with a ramp rate from ambient of 35 °C min^{-1} in an ambient atmosphere (Supplementary Figure S5). The unit-cell length of Ag_2O as a function of time at 100 and 130 °C is shown in Figure 9.

C. Ag_3O unit-cell parameters as a function of temperature

The Ag_3O unit-cell volume as a function of temperature, $V(T)$, for the *in situ* reaction of film 1 is shown in Figure 10 along with the Ag_3O -rich (78 wt%) product of the *ex situ*

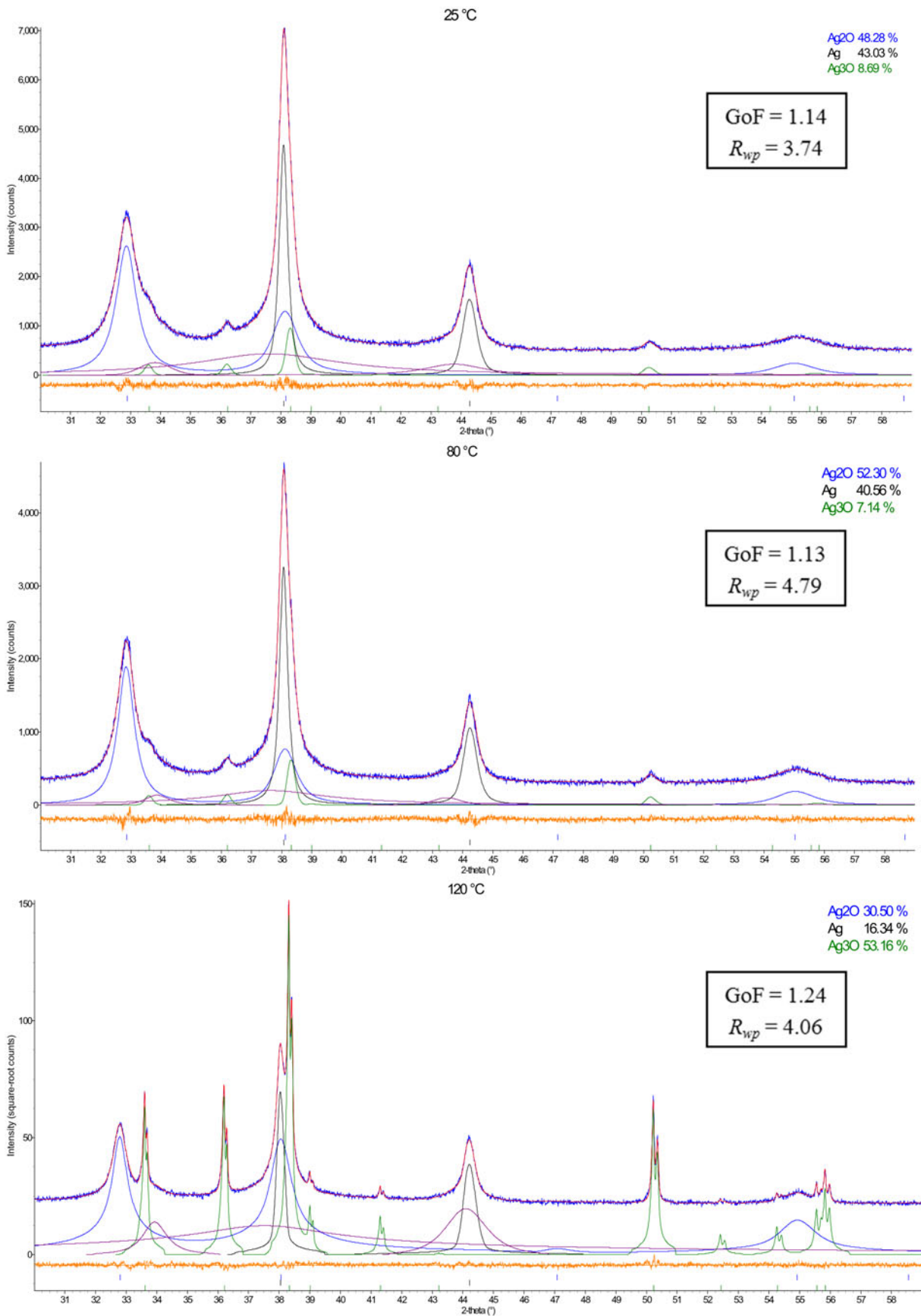


Figure 5. (Color online) Pawley refinements for film 1 heated in N_2 at 25, 80, and 120 °C.

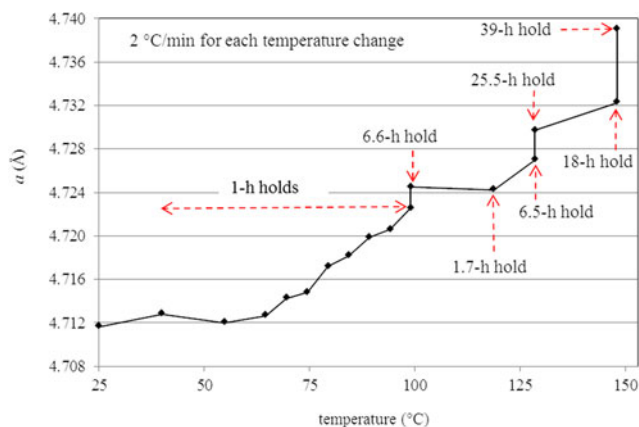


Figure 6. Nonstoichiometric Ag_2O $a(T)$ for the *in situ* reaction of film 1 heated in N_2 . XRPD patterns were collected for the last 15 min of each hold period.

thermal reaction (rxn) of film 1 at 60 °C in air for 1 year (product 1e). The quadratic regression is for product 1e, and the numbers indicate the sequence of the analyses.

Expressing the $V(T)$ for Ag_3O and Ag as a percentage difference of the unit-cell volume at 25 °C allows a relative comparison of their thermal expansion for the *in situ* experiments on film 1 and product 1e (Figure 11). The regression for Ag_3O in Figure 11 was done using data points 1, 2, and 3, and a quadratic function in case data point 4 near 200 °C was decreasing as a function of time during the ramp from low temperature. A decrease in volume with time is clearly observed for point 5. The Ag_3O a and c axes for these two experiments as a function of temperature are shown in Figure 12. The dashed and continuous lines are regressions on a and c , respectively, for product 1e.

The jet-milled films were also reacted *ex situ* at temperatures between 40 and 141 °C in air for up to 1 year (Table II).

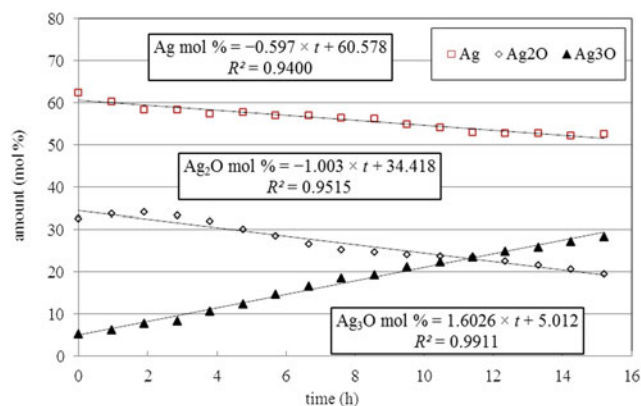


Figure 8. Phase abundance of film 1 at 100 °C in N_2 as a function of time.

The cooling rate for these experiments was only controlled for samples 3a, 3b, and 3c, which were cooled with the same procedure; their cooling rate was unavailable. The Ag_3O $c/a(T)$ is shown in Figure 13 along with the c/a for the *in situ* thermal-reaction experiment described in section III.A.

The c/a for the *in situ* reaction of film 1 from 40 °C to the first 100 °C hold have significantly more uncertainty compared to the c/a from the second 100 °C target to the 150 °C target where the signal from Ag_3O was much higher and the uncertainty of a and c was much less. The relatively high scatter of c/a values is from propagation of errors in c and a combined with the poor reproducibility of determining the position of very weak, convoluted, broad peaks. These data points are graphed with gray circles in Figure 13. The GoFs of these refinements were 1.15 ± 0.05 , and the Durbin Watson d statistic for serial correlation was 1.7 to 1.8, which indicates no strong correlations. The abundances of phases determined in these Pawley refinements varied by about ± 2 wt% for each phase.

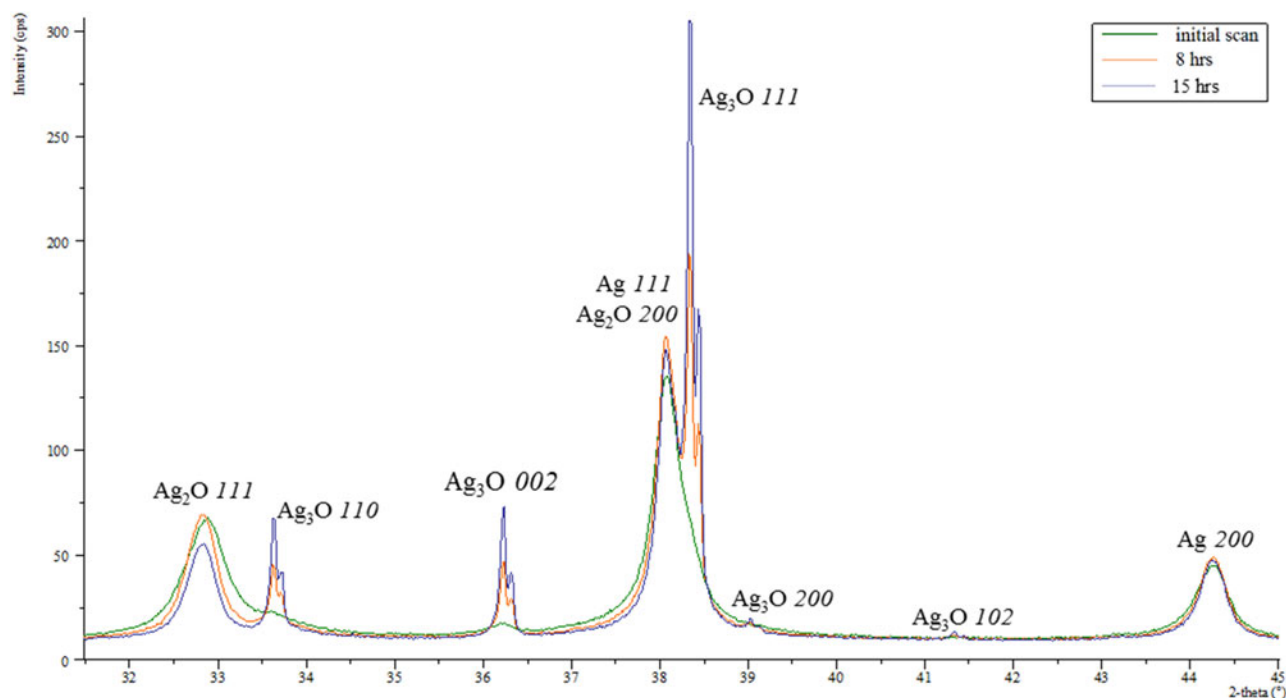


Figure 7. (Color online) Overlays of *in situ* XRPD patterns of film 1 heated at 100 °C in N_2 for 0, 8, and 15 h.

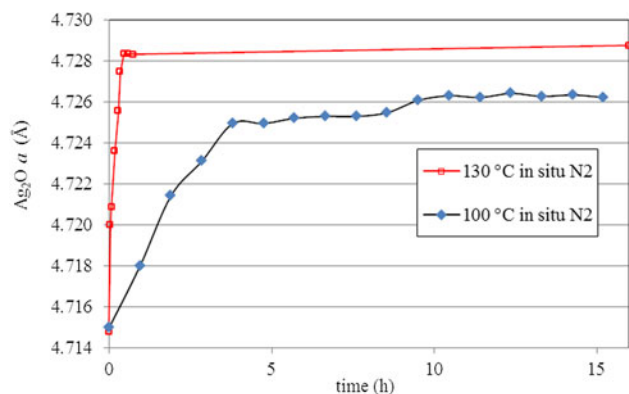


Figure 9. Nonstoichiometric Ag_3O $a(t)$ for the *in situ* reaction of film 1 at 100 and 130 °C in N_2 .

D. *Ex situ* thermal reactions

The *ex situ* thermal-reaction product ID, reaction temperatures, reaction times, reaction atmospheres, and estimated phase compositions are provided in Table II. Ag_3O c/a vs. V for the *ex situ* reaction products at ambient temperature, 24–29 °C, is shown in Figure 14 along with the values from Beesk *et al.* (1981) scaled by the weighted-average $\text{MoK}\bar{\alpha}$ wavelength (0.710782 Å) calculated using the wavelengths of $\text{MoK}\alpha_1$ and $\text{K}\alpha_2$ and their relative intensities from TOPAS (MoKa2.lam) to update the $\text{MoK}\alpha = 0.71069$ Å used by Beesk *et al.* (1981); the scale factor = $0.710782 \div 0.71069 = 1.000130$ and was multiplied by their published unit-cell lengths. The published and scaled values of c/a from Beesk *et al.* (1981) are shown as gray and black squares separated by an arrow, respectively. The c/a for 3c was, within the uncertainty of the refinement, the same as for 3a; it was not graphed in Figures 13 and 14 for clarity. Several other reaction products listed in Table II were not included in the graph because the angle range and resolution of their patterns was too limited for a reliable unit-cell refinement relative to those graphed.

The a axis versus c axis at ambient temperature is shown in Supplementary Figure S7. Some of the whole-pattern refinements are shown in Figures 15 and 16. The very weak $\text{CuK}\beta$ transmitted by the multilayer mirror for the sharp, strong Ag_3O 111 is located at 34.5° ; this peak was not included in the refinements because it did not significantly affect the residual.

E. Ball-milled jet-milled film

The ball-mill experiment produced an estimated 76 wt% of Ag_3O in sample B1 with broad peaks accounted for by an average size (coherence length) and microstrain (ϵ_0) (Figure 16). SRM 640d Si peaks in the pattern were used to define the peak-profile parameters for instrumental resolution. Relatively weak, very broad peaks for the LT Ag_2CO_3 polymorph (Norby *et al.*, 2002) were Pawley refined with an average coherence length = 267(30) Å and $\epsilon_0 = 0.0026(1)$ using a Lorentzian profile. Ag_2O was not detected.

The average coherence length of the Ag_3O in B1 was 280 (2) Å; only a Lorentzian profile component was significant. ϵ_0 was 0.00097(1); only a Gaussian profile was significant. The steep rise of intensity at low angles was small-angle scattering (SAXS) (Figure 16). The origin of the SAXS signal was not investigated and not recorded for most of the patterns in the present study.

Ex situ heating of B1 to 80, 100, and 120 °C in air each linearly decreased the Ag_3O unit-cell volume and abundance (Figure 14; Supplementary Figure S7). On heating to 80 °C, the a axis decreased while the c axis was not significantly different (Supplementary Figure S6), and the SAXS signal decreased by about 80%. Heating to 100 and 120 °C decreased the c axis with essentially no change in the a axis (Supplementary Figure S7). On heating these samples, the coherence length of B1a, B1b, and B1c was 351(5), 395(4), and 479(8) Å, respectively, and ϵ_0 was 0.0007(1), 0.0006(1), and 0.0005(1), respectively. After 5 days at 150 °C, only Ag metal was detected.

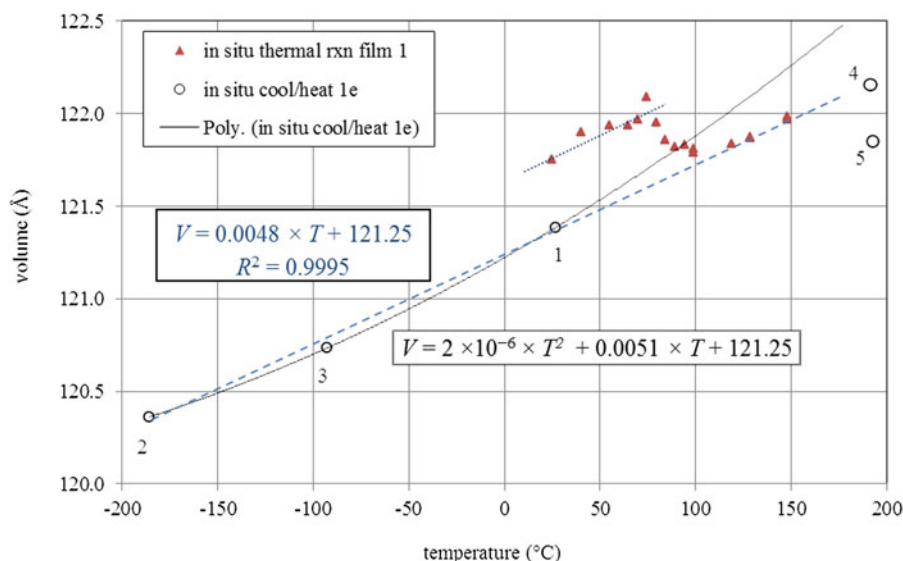


Figure 10. Ag_3O unit-cell $V(T)$ for the *in situ* thermal reaction of film 1 in N_2 starting at ambient temperature and for the *in situ* cooling and heating of product 1e. The time sequence of the cooling and heating of product 1e is indicated by the number next to the data point.

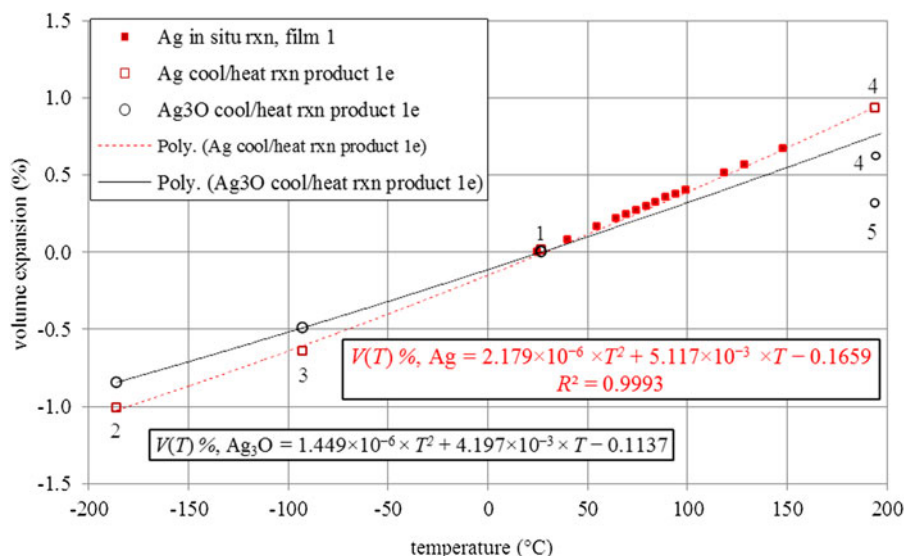


Figure 11. $V(T)$ for Ag_3O and Ag as a percentage difference of their unit-cell volumes relative to 25°C for the *in situ* thermal reaction of film 1 and the *ex situ*, thermal-reaction product 1e. The forward-time sequence for product 1e is indicated by the number next to the data point.

F. Sonicated jet-milled films

The reaction of sonicated films produced an XRPD pattern of Ag_3O with sharper peaks than the Ag_3O peaks from the ball-milled product. LT Ag_2CO_3 has broader Bragg peaks than the Ag_3O . An estimated <1 wt% of Ag_2O remained after both sonication reactions. The products of the cyclohexane sonication for 3 min contained more Ag than the products from sonication in IPA for 45 s (Table II). This might reflect the more reducing nature of cyclohexane compared to IPA.

The Ag_3O c/a for the material synthesized in ball milling and sonication experiments are graphed in Figure 14 but not included in the linear regression because of the strong overlap of several strong peaks for Ag_3O and Ag_2CO_3 (Supplementary Figures S8 and S9) which could affect the accuracy of their unit-cell parameters. The peak broadening for Ag_2CO_3 was

significantly anisotropic; this was not included in the structural model. Therefore, the unit-cell parameters of Ag_2CO_3 could be less accurate compared to the parameters from the Pawley refinements of the patterns displaying very sharp peaks of Ag_3O with mostly instrumental and isotropic broadening.

IV. DISCUSSION

A. Diffuse scattering: Ag_2CO_3 and stacking faults in Ag

Diffuse peaks were used as background in the whole-pattern refinements to facilitate the best fit to the Bragg peaks and maximize the accuracy of the unit-cell parameters. One of the diffuse peaks ranged between 42 and 45° (Figure 5) and was used to fit the asymmetry of the $\text{Ag } 200$ hkl which has

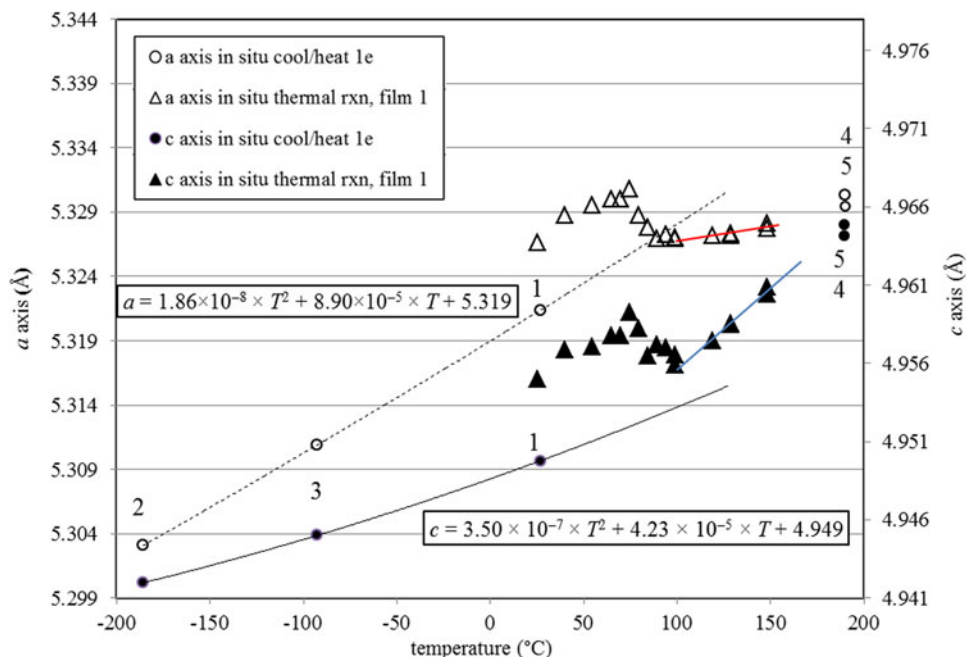


Figure 12. The a axis and c axis of Ag_3O as a function of temperature for the *in situ* thermal reaction of film 1 heated in N_2 and the *in situ*, cooling and heating of thermal-reaction product 1e. The regression lines are for the cooling of product 1e and are extrapolated to higher temperatures.

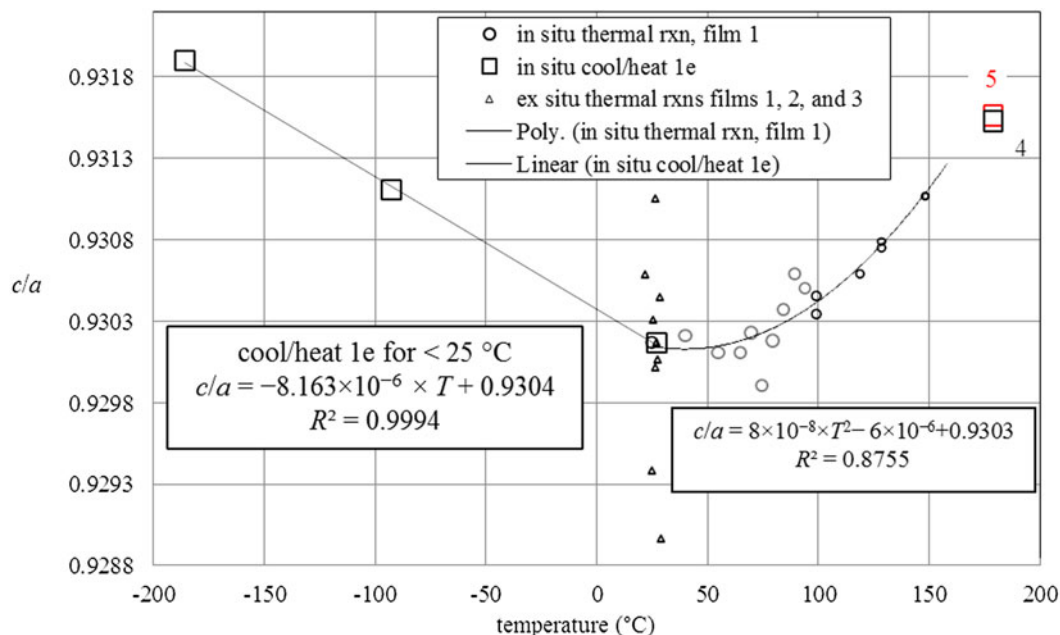


Figure 13. The $c/a(T)$ for Ag_3O produced by *in situ* and *ex situ* thermal reactions. The numbers next to the markers for product 1e indicate the time sequence of the analyses.

a low-angle tail. The tail is a consequence of a reciprocal-lattice intensity rod generated by stacking faults (Schields *et al.*, 2007). A characteristic peak generated by stacking faults in Ag starts at about 36° and extends several degrees to lower angles; this saw-toothed peak was too weak to detect. The Ag stacking-fault probabilities for many patterns in the present study were refined using the Warren model in MAUD 1.999 (Lutterotti *et al.*, 1999) which accounts for the 200 tail. The probabilities were in the range of several tenths of a percent.

Weak, diffuse scattering with a maximum ranging from 33.7 to 34.1° was present in all of the Ag_3O -rich patterns. The width (FWHM) of this maximum decreases continuously as a function of temperature (Supplementary Figure S10) for

the *in situ* thermal reaction of film 1 and products 1d and 3b. The net intensity of this maximum is approximately constant as a function of temperature for the *in situ* thermal reaction of film 1. If this peak was from thermal-diffuse scattering by acoustic phonons in Ag_3O , we expect it would increase its intensity with increasing temperature. We hypothesize this peak is from metastable $\beta\text{Ag}_2\text{CO}_3$, one of the high-temperature forms, which has two relatively intense peaks very near the position of this diffuse-scattering maximum that merge into one peak with a maximum of 33.76° when broadened. The next strongest peaks for $\beta\text{Ag}_2\text{CO}_3$ are near 19.34 and 48.51° . The Pawley fit of the pattern of the ball-milled sample, which was rich in LT Ag_2CO_3 , required weak peaks near these

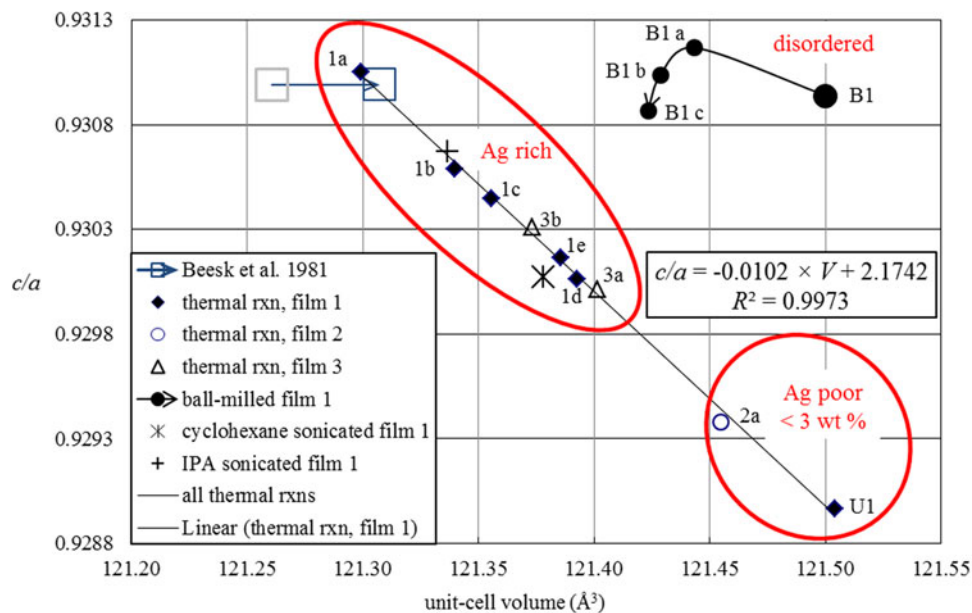


Figure 14. The Ag_3O c/a at room temperature for the products of *ex situ* thermal reactions, ball milling, and sonication reactions as a function of unit-cell volume. The data from Beesk *et al.* (1981) (gray square) were measured on a single crystal hydrothermally synthesized on Ag metal and were scaled using MoK α from TOPAS as shown by the arrow from the gray square to the black square.

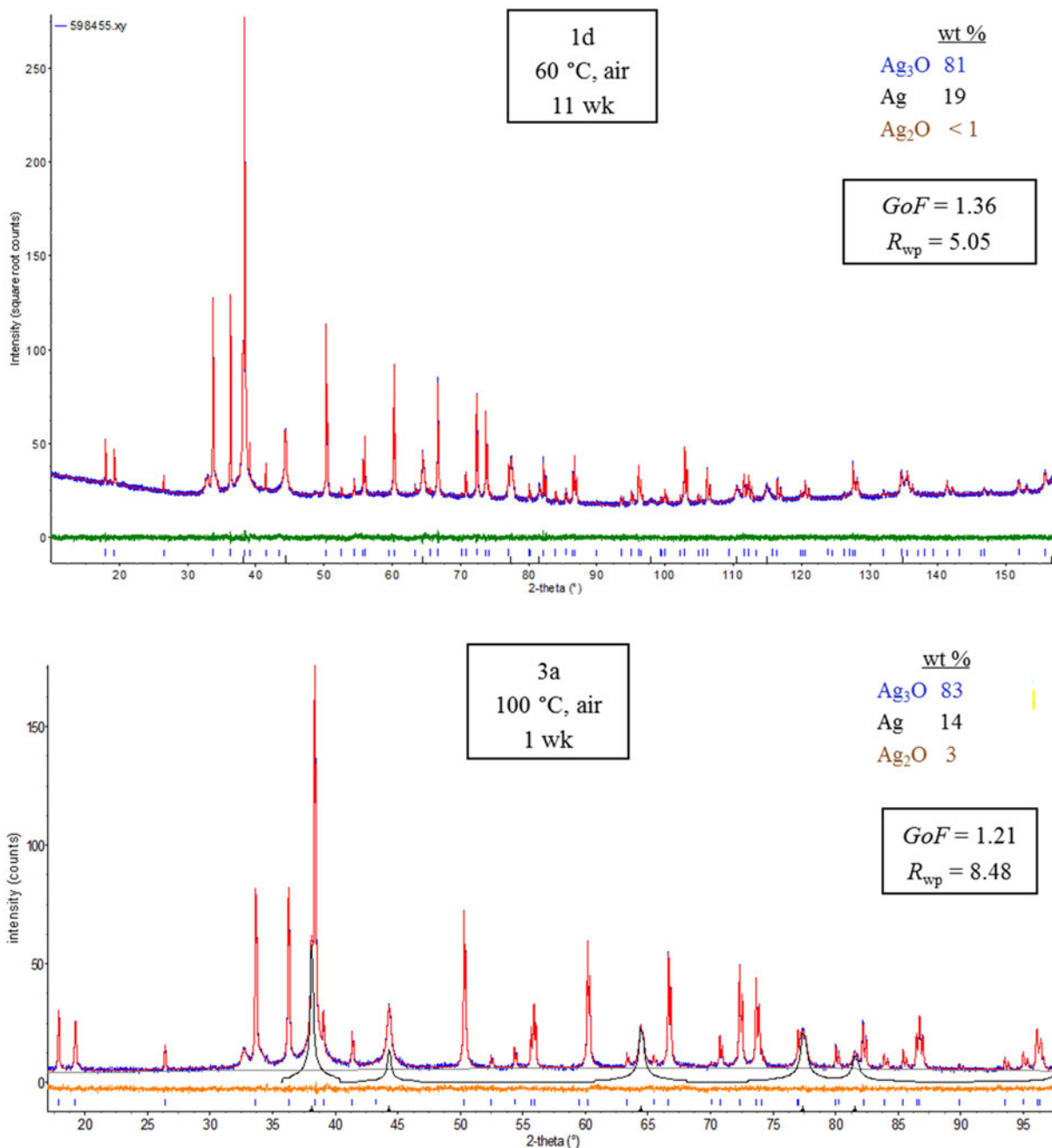


Figure 15. (Color online) TOPAS Pawley refinements for products 1d and 3a. The color-coded tick marks correspond to the color-coded formulas for Ag₃O and Ag.

three presumed β Ag₂CO₃ peak positions. However, the peaks from β Ag₂CO₃ are much too weak and broad to determine the unit-cell parameters. Norby *et al.* (2002) determined its unit-cell parameters at 180 °C.

Another very diffuse peak centered at $\sim 37.5^\circ$ is included in most of the Pawley refinements on patterns of samples containing at least a minor amount of Ag₂O. Ag₂O is known to readily form Ag₂CO₃ when exposed to an atmosphere containing CO₂; however, crystalline Ag₂CO₃ was only detected in trace amounts in the thermal-reaction products. We hypothesize Ag₂CO₃ forms a very thin layer on Ag₂O (Culbertson, 1964) starting at ambient conditions, and, unless the layer is removed, the rate of formation decreases with time. Fresh Ag₂O surfaces were being created during the ball-mill and sonication experiments, which produced abundant crystalline

LT Ag₂CO₃ presumably from reaction of Ag₂O and ambient CO₂. We are unsure of the identity of this peak.

B. Thermal reaction of jet-milled films

All of the phases in film 1 displayed broad Bragg peaks indicating the presence of disorder, which was modeled using crystallite size and microstrain. The values of size and strain are not meaningful because of the short range of 2θ and the inaccuracies of refining very broad, weak peaks at higher angles. The parameters of size and strain facilitated the best fit to the Bragg peaks.

The abundances of the phases remained constant until $\sim 80^\circ\text{C}$ (Figure 4); at 99°C , the abundance of Ag₃O significantly increased from ~ 8 to ~ 50 wt%. From 129 to 148°C , the amount of Ag₃O begins to decrease, and the amount of

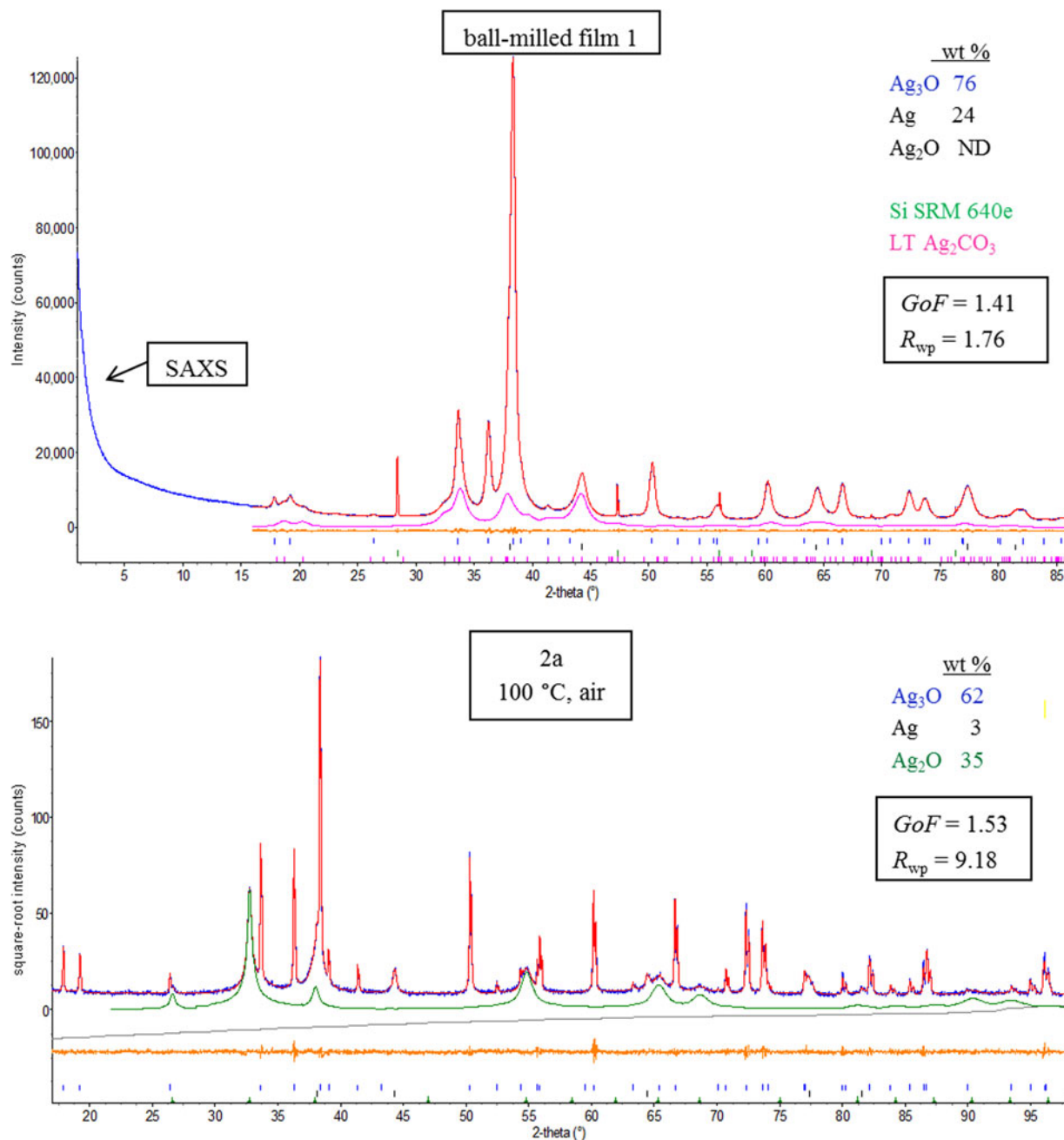


Figure 16. (Color online) TOPAS Pawley refinements for ball-milled film 1 and product 2a. The color-coded tick marks correspond to the color-coded phases detected.

Ag increases; this indicates Ag_3O is decomposing to Ag. The Ag_3O unit-cell volume decreases with time at 148°C (section IV.D.1) while decomposing to Ag.

The kinetics and extent of the thermal reaction of Ag and Ag_2O depend on the heating rate. For example, if the temperature is increased at $35^\circ\text{C min}^{-1}$ from ambient temperature to 130°C , only the initial 8 wt% Ag_3O with sharper peaks is detected after 41 h. Other examples of the dampened reaction with relatively high heating rates were also observed.

C. Kinetics of the thermal reaction to form Ag_3O at 100°C and 130°C

The estimated phase abundance of film 1 heated to 100°C in N_2 as a function of time (Figure 7) shows the reaction rates

are constant (Figure 8). The Ag_2O reaction rate, $-1.003 \text{ mol}\% \text{ h}^{-1}$, is 68% faster than Ag, $-0.597 \text{ mol}\% \text{ h}^{-1}$. For stoichiometric Ag_2O and Ag_3O , the reaction rate for Ag and Ag_2O to form Ag_3O must be equal because the reactants combine in equimolar ratio. This difference in reaction rates is readily apparent in the Ag 200 peak, which decreases intensity very little compared to the Ag_2O 111 peak as the reaction proceeds (Figure 7); this can also be seen in Figure 2.

The difference in reaction rates indicates nonstoichiometry in Ag_3O and/or Ag_2O . For example, if Ag_2O is oxygen deficient and Ag_3O is stoichiometric, its formula would be $\text{Ag}_2\text{O}_{1-x}$ with $x=0.17$ to balance the reaction. If Ag_2O is stoichiometric, then the silver suboxide would be oxygen rich, $\text{Ag}_3\text{O}_{1+x}$ with $x=0.15$. Linear combinations of these compositional end members are possible. Analogous examples

could be cast with a variable silver stoichiometric coefficient and stoichiometric oxygen content.

Both film 1 and film 3 reactants started with about the same Ag/Ag₂O molar ratio of two. If the rates are constant for the thermal reactions of these films, Ag₂O would be depleted in 34 h with 17.5 wt% remaining Ag and 82.5 wt% Ag₃O produced. These predicted amounts are very close to the amounts measured with *ex situ* thermal-reaction experiments at 100 °C shown in Table II for products, 1b (48 h), 3a, and 3b: 84, 83, and 81 wt% Ag₃O, respectively. This observation indicates the constant reaction rate largely persisted in 1b until the limiting reactant Ag₂O was almost depleted. An almost constant rate indicates the reactants remain readily available to each other, the reactivity of the reactants remains constant, and diffusion is not limiting the reaction.

The kinetics and extent of the thermal reaction of Ag and Ag₂O depend on the heating rate. The thermal reaction was not detected in film 1 after ramping to 130 °C at 35 °C min⁻¹ (Supplementary Figure S5). The only change after 41 h was the sharpening of the Ag₂O and Ag₃O peaks.

D. Ag₃O unit-cell parameters

1. V(T)

The unit-cell volume of the starting disordered Ag₃O in film 1 increased with about the same slope (Figure 10, dotted line) as the ambient to low-temperature linear slope of V(T) for product 1e extrapolated to higher temperatures (Figure 10, dashed line). From 119 to 148°, the Ag₃O unit-cell volume of film 1 increases with about the same slope as the linear regression for the low-temperature expansion of product 1e extrapolated from 25 to 122 °C (Figure 10, dashed line). This volume expansion of product 1e is significantly different than the quadratic regression of the low-temperature expansion of film 1 (Figure 10, solid line). However, sparse data points over these ranges preclude the distinction between linear and quadratic volume expansion of Ag₃O in both samples.

Figure 11 compares the volume expansion of Ag₃O and Ag measured in these same *in situ* experiments of film 1 and product 1e. The expansion of Ag₃O is about 80% less than Ag over the entire measured range. The close agreement of the Ag volumes measured in these separate *in situ* experiments indicates the determined unit-cell parameters have repeatability adequate for comparison between experiments. Suh *et al.* (1988) showed their measured thermal expansion of Ag, Au, Cu, and Ni by XRPD and dilatometry from 25 °C to at least 1000 °C was modeled well by a quadratic equation with positive curvature, and their results were consistent with the data from several previous studies. Many closest-packed structures have thermal expansion with positive curvature (Iwanaga *et al.*, 2000). Distinguishing between linear and quadratic functions for the thermal expansion of Ag₃O requires many more data points throughout the temperature ranges of interest than were collected in the present study.

The volume of Ag₃O in film 1 decreases 0.2% from 79 to 94 °C when the thermal reaction of Ag and Ag₂O starts to form Ag₃O. This volume decrease could be due to the Lorentz effect described by Öztürk *et al.* (2015) if the size of the crystal prior to the thermal reaction was < 100 Å and

the size increases from 79 to 94 °C. The short 2θ range, broad peaks, and weak signal preclude the refinement of size and microstrain for patterns in this temperature interval.

2. a(T) and c(T)

Figure 12 shows the Ag₃O *a* axis and *c* axis expansions from ambient to low temperatures display a slight positive curvature as reflected in its volume expansion. Their expansions are anisotropic with the *a* axis slope and absolute change about twice those of the *c* axis from -162 to 25 °C. The lengths of the *a* and *c* axes show an abrupt decrease from 80 to 95 °C as expected from the corresponding abrupt volume decrease. The *c* axis then continues to increase with about the same or slightly increased initial slope while the *a* axis is approximately constant as temperature rises, a striking difference.

The *c/a(T)* for Ag₃O produced by *in situ* thermal reactions (Figure 13) shows a negative, linear slope (-8.163 × 10⁻⁶ C⁻¹) for *T* ≤ ambient. This slope is compared to the *c/a(T)* slope of -2 × 10⁻⁵ C⁻¹ for Ag₂F (Williams, 1989), which has a structure similar to Ag₃O except the octahedral interstices in the cp Ag bilayers are *all* occupied by F in every other adjacent bilayer. The linearity of *c/a(T)* is a consequence of a frozen-in anisotropy of *a* (*T*) and *c*(*T*). The inversion of *c/a(T)* near ambient *T* reflects the decrease in the expansion of the *a* axis, while the expansion of the *c* axis continues to increase with increasing temperature above ambient *T* (Figure 12). Between 194 and 293 °C, the Ag₃O in product 1e completely transformed to Ag and Ag₂O.

3. c/a vs. V at ambient T

The *c/a* ratios vs. volume (*c/a* vs. *V*) at ambient *T* for the *ex situ* thermal-reaction products (Table II), ball-milling product, and sonication products are shown in Figure 14. The linearity of *c/a* vs. *V* for the thermal-reaction and sonication products indicates a dependence on a compositional variable and/or variable state of disorder; both are expected to change *c/a* vs. *V*. We presume the single-crystal studied by Beesk *et al.* (1981) was in equilibrium with Ag during their several-day, hydrothermal synthesis. The phase composition of the products reveals samples with <3 wt% Ag and excess Ag₂O (Ag poor), and a Ag-rich group with excess Ag and almost no detectable Ag₂O as encircled in Figure 14. This trend suggests the redox potential associated with solid-solid contacts is a factor determining the position along the linear relation.

Ag-rich phase compositions of the reaction products are expected to be most reducing and associated with oxygen-poor nonstoichiometric Ag₃O with a relatively smaller unit-cell volume. Ag-poor compositions are expected to be relatively oxidizing and associated with oxygen-rich nonstoichiometric Ag₃O with a relatively larger unit-cell volume.

The heating and cooling rates of samples 3a and 3b were controlled to be the same; the atmosphere was air for both. The only difference between the thermal-reaction conditions for this pair is the one-week longer time at 100 °C for 3b. We hypothesize the smaller volume and increase of *c/a* of 3b relative to 3a was caused by the loss of oxygen rather than a possible change in order and disorder generated by temperature. If this hypothesis is correct, the increase of *c/a* (*V*) could be extrapolated to explain the inversion of the *c/a* (*T*) above

ambient (Figure 13) as a loss of oxygen with increasing temperature in the *in situ* thermal reaction of film 1. The same reasoning applies for points 4 and 5 observed for the heating of product 1e where the *c/a* increases and unit-cell volume decreases with time at 194 °C.

a Ex situ heating of ball-milled sample

The *c/a* (*V*) for the ball-milled samples (Figure 14) are significantly removed from those fit with a linear function, and they display broad Bragg peaks. The broadening was mostly generated by short coherence lengths (crystal size) rather than microstrain. The other samples in Figure 14 all have sharp Bragg peaks with essentially no intrinsic peak broadening. We consider the possibility of the refined unit-cell parameters being affected by a Lorentz correction (Öztürk *et al.*, 2015) which significantly biases the position of Bragg peaks to lower Bragg angles and larger *d*-space for crystals < 100 Å in size. Our refined estimate of the average coherence length, 225(5) Å, in the ball-milled sample is expected to be too large to cause a significant bias to larger *d*-spaces and corresponding unit-cell volumes.

The continuous drop in unit-cell volume on heating the ball-milled sample and the corresponding linear increase of the Ag content is consistent with Ag₃O decomposing to Ag metal by volatilizing oxygen. The volume change during the first heating at 80 °C was almost completely from the decrease in the *a* axis. Subsequent volume changes at 100 and 120 °C were mostly from a decrease in the *c* axis. The increase of size and decrease in microstrain with increasing temperature-time treatments is consistent with crystal growth and a decrease in disorder. However, these microstructural changes are relatively small.

E. Ag₂O *a*(*T*) and *a*(*t*)

The Ag₂O *a*(*T*) (Figure 6) shows the effect of negative thermal expansion (Tiano *et al.*, 2003) and kinetic changes in composition due to nonstoichiometry and thermal equilibration. The almost flat to negative change at the start of heating from ambient and the 1.7 h hold at 120 °C reveal the negative thermal expansion because the kinetics of compositional changes for these temperatures and hold times are slow relative to the other temperature/time steps.

The large 0.57% expansion of volume over the range shown in Figure 6 is hypothesized to be driven by a decrease in nonequilibrium volume-contracting point defects, which impart nonstoichiometry. Equilibration of these point defects is kinetic as shown in Figure 9 at 100 and 130 °C. The expansion rate from 65 to 100 °C is fast enough to mask the decrease of *a* from thermal expansion. After the first 100 °C hold, the volume increases much slower. We have characterized this equilibration in Ag₂O made with significantly different processes including powders made from as-removed thin films in the present study without jet milling and an as-deposited Ag–Ag₂O magnetron-sputtered thin films (Figure 17).

The expansion of Ag₂O with increasing temperature was characterized *ex situ* by Faivre (1940), Allen (1960), Kato and Anju (1972), and Taylor *et al.* (2005) (Supplementary Figure S12). Ag₂O films synthesized with oxidizing conditions by Wei *et al.* (2011) were determined to have oxidation states of Ag higher than 1⁺ by X-ray photoelectron

spectroscopy, and the corresponding point defects were especially volume contracting (Figure 17).

The Ag–Ag₂O thin film studied by Taylor *et al.* (2005) was synthesized with conditions similar to the thin films of the present study and was found to have a relatively low volume which increased rapidly with mild heating. The Ag₂O in these films decomposes completely to Ag metal by 110 °C. We hypothesize the Ag₂O films characterized by Wei *et al.* (2011) have excess oxygen. The volume increase from the point defects associated with excess oxygen is more than offset by the significant volume contraction from point defects associated with Ag²⁺ and Ag³⁺. These hypothetical point defects are likely to be clusters of excess oxygen and higher oxidation states of Ag.

F. SEM photomicrographs of thermal-reaction products

Supplementary Figure S11(a) shows a scanning electron microscopy (SEM) photomicrograph of Ag₃O crystals with some facets produced by the thermal reaction of a jet-milled film. The reaction temperature for this product was between 40 and 100 °C; the time period is unavailable. The smaller irregular particles and warty, faceted crystals imbedded in the larger crystal look like they are merging with the larger faceted crystal. This morphology contrasts the irregular and rough morphologies of the *in situ* thermal reaction described in section III.A heated to 148 °C for 39 h and product 1e [Supplementary Figures S11(b) and S11(c)].

G. Ag₃O tunnel structure

The Ag₃O structure determined by Beesk *et al.* (1981) consists of a sublattice of distorted hcp Ag with a two-layer repeat and oxygen occupying two-thirds of the octahedral interstices in every other adjacent cp layers (Figure 1). The Ag in cp layers occupied by oxygen are expanded from their perfect hcp positions, and the Ag₆O octahedra have three adjacent, empty octahedral interstices. These empty octahedral interstices share rotated trigonal Ag₃ faces along the *c* axis shown in Figure 1(b) as two equilateral triangles (blue) rotated by 60° around their common center point. The empty octahedra form a continuous, trigonal tunnel of space through the trigonal planar Ag (Ag–Ag 2.86 Å), which are 1.65 Å from the tunnel axis; this “tunnel radius” is slightly larger than the effective radius of 1.40 Å for O²⁻ and the effective radius of 1.445 Å for ccp Ag metal. These empty interstices also form rows coincident with the *a* axis and *c* axis in the oxygen-coordinating Ag cp bilayer. The tunnels are a modality for high ionic conductivity of oxygen and silver as well as a readily available diffusion path. The tunnels also provide a connection between the Ag bilayers occupied by oxygen and the Ag bilayers unoccupied by oxygen.

H. Variable oxygen content of nonstoichiometric Ag₃O analogs

The crystal structure of Ag₃O reported by Beesk *et al.* (1981) was refined using anisotropic thermal-displacement parameters; however, these parameters were not published. These authors do not report they explored the possibility of variable occupancy of oxygen in the ordered octahedral site

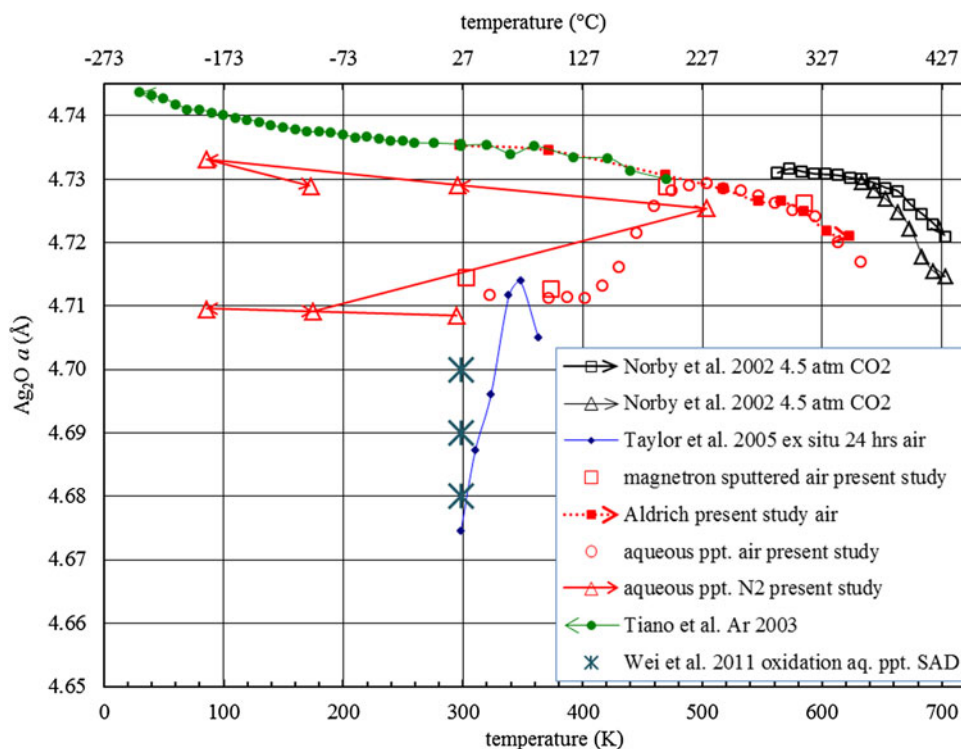


Figure 17. (Color online) Ag_3O $a(T)$ from several studies and the present study. The values for Taylor *et al.* (2005) were graphed at their annealing temperatures by adding the thermal expansion determined by Tiano *et al.* (2003).

and the disordered occupation of oxygen in the layer of nominally unoccupied interstices.

Several metal suboxide structures with variable occupation of oxygen in the octahedral interstices of the close-packed metal sublattice are published for Ti, Zr, and Hf (Banerjee and Mukhopadhyay, 2007). Hirabayashi *et al.* (1973) reported *ex situ* high-temperature experiments in the Hf–O system with 10–20% atomic oxygen. The unit-cell parameters of these samples were measured with XRPD. For the composition close to the Hf_6O stoichiometry and space group $P\bar{3}1c$, the structure has oxygen in every cp bilayer. They found the unit-cell volume and the c/a increased with increasing oxygen. Using single-crystal neutron diffraction, they determined oxygen has an ordered and variable occupation of octahedral interstices as a function of temperature. When Hf_6O was quenched from 1000 °C, the oxygen occupancy was disordered and increased the volume by 0.6% relative to the ordered structure with the same oxygen content.

The Ag_3O unit-cell volume of film 1 (Figure 10) decreases by 0.2% from 80 to 95 °C when the reaction to produce more Ag_3O begins to be detected. If the Lorentz effect discussed in section IV.D.1 is not a significant cause of this decrease, we hypothesize this volume decrease is due to a change in the amount of oxygen and/or the order/disorder of the oxygen. The disorder could be interstitial oxygen occupying the vacant octahedral interstice of the perfect structure, vacant oxygen in the octahedral interstice of the perfect structure, and disordered oxygen in the octahedral interstices of the Ag bilayers which are all vacant in the perfect structure. The presence of planar stacking disorder of the silver and oxygen cp layers provides many possible scenarios with respect to their influence on the nonstoichiometric composition. These

scenarios might also lead to the outlying Ag_3O volume produced by ball milling and subsequent heating (Figure 14).

I. Qualitative model for the range of c/a in Ag_3O

The suite of Ag_3O -rich samples with a linear c/a vs. V is hypothesized to have a continuously variable amount of oxygen in the ordered oxygen layer of the perfect structure. The c/a is an additive measure of distortion generated by oxygen, and V is an additive measure of the total amount of oxygen. We hypothesize the linear relation between c/a and volume in Figure 14 and the inversion of c/a above room temperature in Figure 13 are generated by changes in oxygen composition and disordering.

XRPD is relatively insensitive to the 4.7 wt% oxygen in stoichiometric Ag_3O , even from relatively large changes in oxygen composition. This insensitivity combined with a high correlation between thermal-displacement parameters and site occupancy obscures the accurate refinement of these variables using XRPD data. We defer to prospective neutron diffraction analysis, which has high sensitivity to oxygen, to determine the origin of c/a (V) at constant temperature and the inversion of c/a above ambient temperature in Figure 13.

V. CONCLUSION

A suite of nonstoichiometric Ag_3O -rich samples was synthesized by mild heating, sonication, and ball milling of jet-milled Ag– Ag_2O magnetron-sputtered films in air and N_2 at ambient pressure. The phase composition, unit-cell parameters, and reaction rates for thermal transformation of the films indicate Ag_3O was produced from the reaction of nonstoichiometric Ag_2O and ccp Ag.

The variation of the Ag_3O unit-cell volumes and c/a as a function of temperature indicates Ag_3O has a range of nonstoichiometric compositions. The nonstoichiometry is likely a consequence of the oxygen content and the ordering of oxygen in the octahedral interstices of the hcp Ag sublattice. Ag_3O is metastable and decreases its unit-cell volume during kinetic decomposition to Ag when heated above ambient temperature in air and nitrogen.

The thermal volume expansions of Ag and Ag_3O below room temperature have similar positive curvature. The relative thermal expansion of Ag_3O is less than Ag by about 80% at room temperature and below. The thermal expansion of Ag_3O is anisotropic; expansion along the a axis is about twice the expansion along the c axis. This results in a decrease of c/a with increasing temperature below room temperature. Above room temperature, the $c/a(T)$ makes a remarkable inversion of slope due to the decrease of the a -axis expansion to near zero and an increase in the c -axis expansion. The suite of nonstoichiometric Ag_3O samples displays a linear relation between c/a and unit-cell volumes at room temperature. The linear relation is hypothesized to be partly controlled by the redox potential of the system and oxygen content of Ag_3O . The site occupancy of oxygen in Ag_3O is most suited to neutron diffraction analysis.

SUPPLEMENTARY MATERIAL

The supplementary material for this article can be found at <https://doi.org/10.1017/S0885715620000561>.

ACKNOWLEDGEMENTS

The authors acknowledge Stephan X.M. Boerrigter and Patrick A. Tishmack, AMRI WLF, for review and discussion.

- Allen, J. A. (1960). "Thermal decomposition of silver (I) oxide," *Aust. J. Chem.* **13**, 431–442.
- Banerjee, S. and Mukhopadhyay, P. (2007) "Interstitial ordering," in *Phase Transformation: Examples from Titanium and Zirconium Alloys*, edited by R. W. Cahn (Elsevier Science, Amsterdam, The Netherlands), Vol. **12**, pp. Chapter 8, pp. 719–781.
- Beesk, W., Jones, P. G., Rumpel, H., Schwarzmann, E., and Sheldrick, G. M. (1981). "X-ray crystal structure of Ag_6O_2 ," *J. Chem. Soc., Chem. Commun.*, 664–665.
- Birkenberg, B. and Schwarzmann, E. (1974). "Zuchtung von Ag_2O -Kristallen unter hydrothermalen Bedingungen," *Z. Naturforsch.* **29b**, 113–114.
- Bruker-AXS (2009). TOPAS V4.2, "General profile and structure analysis software for powder diffraction data," User's Manual, Bruker-AXS 5465 Karlsruhe, Germany.
- Culbertson Jr., W. J. (1964). "Investigation and design of a regenerable silver oxide system for carbon dioxide control," Denver Research Institute, AMRL-TR-64-119.
- Faivre, R. (1940). "Formation de solutions d'insertion au cours de la dissociation de l'oxyde d'argent," *Compt. Rend. Hebd. Seances Acad. Sci.* **210**, 398–400.

- Hirabayashi, M., Yamaguchi, S., and Arai, T. (1973). "Superstructure and order-disorder transformation of interstitial oxygen in Hafnium," *J. Phys. Soc. Japan* **35**(2), 473–481.
- Hölzer, G., Fritsch, M., Deutsch, M., Härtwig, J., and Förster, E. (1997). " $K\alpha_{1,2}$ and $\beta K_{1,3}$ X-ray emission lines of the 3d transition metals," *Phys. Rev. A* **56**, 4554–4568.
- Iwanaga, H., Kunishige, A., and Takeuchi, S. (2000). "Anisotropic thermal expansion in wurtzite-type crystal," *J. Mat. Sci.* **35**, 2451–2454.
- Kabalikina, S. S., Popova, S. V., Serebryanaya, N. R., and Vereshchagin, L. F. (1963). "A new modification of Ag_2O with a layer structure," *Sov. Phys. - Dokl.* **8**, 972.
- Kato, A. and Anju, Y. (1972). "Expansion of Ag_2O lattice by annealing," *J. Am. Ceram. Soc.* **55**, 25–28.
- Kern, A., Coelho, A. A., and Cheary, R. W. (2004). "Convolution based profile fitting," in *Diffraction Analysis of the Microstructure of Materials*, edited by E. J. Mittemeijer and P. Scardi, Materials Science (Springer), pp. 17–50.
- Kosova, D. A., Emelina, A., and Bykov, M. (2014). "Phase transitions of some sulfur-containing ammonium salts," *Thermochim. Acta* **595**, 61–66.
- Lutterotti, L., Matthes, S., and Wenk, H.R. (1999). "MAUD (Materials analysis Using Diffraction): a user friendly Java program for Rietveld Texture Analysis and more," in *Proceeding of the Twelfth International Conference on Textures of Materials* (NRC Research Press, Ottawa, Canada), Vol. 1, p. 1599.
- Norby, P., Dinnebier, R., and Fitch, A. N. (2002). "Decomposition of silver carbonate; the crystal structure of two high-temperature modifications of Ag_2CO_3 ," *Inorg. Chem.* **41**, 3628–3637.
- Nordman, C. E. and Schmitkons, D. L. (1965). "Phase transition and crystal structures of adamantane," *Acta Cryst.* **18**, 764–767.
- Öztürk, H., Yan, H., Hill, J. P., and Noyan, I. C. (2015). "Correlating sampling and intensity statistics in nanoparticle diffraction experiments," *J. Appl. Cryst.* **48**, 1212–1227.
- Pawley, G. S. (1981). "Unit-cell refinement from powder diffraction scans," *J. Appl. Cryst.* **14**, 357–361.
- Schields, P. J., Dunwoody, N., Mamak, M., Gendron, C., and Bates, S. (2007). "Comparison of simulated and experimental XRPD patterns of silver with twin faults using MAUD and DIFFaX," *Adv. X-ray Anal.* **51**, 162–168.
- Schlemper, E. O. and Hamilton, W. C. (1966). "Neutron-diffraction study of the structures of ferroelectric and paraelectric ammonium sulfate," *J. Chem. Phys.* **44**, 4498–4509.
- Suh, I., Ohta, H., and Waseda, Y. (1988). "High-temperature thermal expansion of six metallic elements measured by dilation method and X-ray diffraction," *J. Mat. Sci.* **23**, 757–760.
- Taylor, P. L., Omotoso, O., Wiskel, J. B., Mitlin, D., and Burrell, R. E. (2005). "Impact of heat on nanocrystalline silver dressings. Part II: Physical properties," *Biomaterials* **26**, 7230–7240.
- Tiano, W., Dapiaggi, M., and Artioli, G. (2003). "Thermal expansion in cuprite-type structures from 10 K to decomposition temperature: Cu_2O and Ag_2O ," *J. App. Cryst.* **36**, 1461–1463.
- van Ekeren, P. J., van Genderen, A. C. G., and van den Berg, G. J. K. (2006). "Redetermination of the thermodynamic properties of the solid-solid transition of adamantane by adiabatic calorimetry to investigate the suitability as a reference material for low-temperature DSC-calibration," *Thermochim. Acta* **446**, 33–35.
- Wei, W., Mao, X., Ortiz, L. A., and Sadoway, D. R. (2011). "Oriented silver oxide nanostructures synthesized through a template-free electrochemical route," *J. Mat. Chem.* **21**, 432–438.
- Williams, A. (1989). "Neutron powder diffraction study of silver subfluoride," *J. Phys. Condens. Matter* **1**, 2569–2574.
- Yoder-Short, D. (1993). "On a small error in SRM640, SRM640a and SRM640b lattice parameters," *J. Appl. Cryst.* **26**, 272–276.